*Journal of The Electrochemical Society*, 2023 **170** 080521

# Investigating Dry Room Compatibility of Chloride Solid-State Electrolytes for Scalable Manufacturing

**Yu-Ting Chen,[1] Darren H. S. Tan,[2] So-Yeon Ham,[1] Baharak Sayahpour,[1] Jeong Beom Lee,[3] Yeeun Kim,[3] Min-Sang Song,[3] Long Hoang Bao Nguyen,[2] Jin An Sam Oh,[2] Phillip Ridley,[2] Ashley Cronk,[1] Grayson Deysher,[1] Jihyun Jang,[2,4,z] Zheng Chen,[1,2,5,6,z] and Ying Shirley Meng[1,2,5,7,z]**

[1]*Program of Materials Science and Engineering, University of California San Diego, La Jolla, California 92093, United States of America*
[2]*Department of NanoEngineering, University of California San Diego, La Jolla, California 92093, United States of America*
[3]*LG Energy Solution, Ltd., LG Science Park, Magokjungang 10-ro, Gangseo-gu, Seoul 07796, Korea*
[4]*Department of Chemistry, Sogang University, Mapo-Gu, Seoul 04107, Korea*
[5]*Sustainable Power & Energy Center (SPEC), University of California San Diego, La Jolla, California 92093, United States of America*
[6]*Program of Chemical Engineering, University of California San Diego, La Jolla, California 92093, United States of America*
[7]*Pritzker School of Molecular Engineering, The University of Chicago, Chicago, IL 60637, United States of America*

Solid-state electrolytes (SSEs) are receiving growing attention as they can replace conventional organic liquid electrolytes to alleviate flammability issues. The low Young's modulus, decent ionic conductivity, and good oxidation stability make chloride SSEs promising candidates to be used as catholytes in all-solid-state batteries. To assess the scalability of chloride SSEs, their chemical stability in air and dry room environments needs to be evaluated. In this study, threechloride SSEs are investigated for their chemical stability under ambient air and dry room conditions: $Li_2ZrCl_6$ (LZC), $Li_3YCl_6$ (LYC), and $Li_3InCl_6$ (LIC). LZC undergo an irreversible hydrolysis reaction during air exposure and cannot be recovered by heat treatment. LYC decomposes into its hydrated precursors when exposed to ambient air, and further hydrolyzed during heat treatment and was thus not recoverable. LIC forms a stable hydrate and can be easily recovered by heating at 260 °C under vacuum. Finally, the electrochemical performance of dry room exposed chloride SSEs is evaluated where capacity loss was observed due to the lower SSE ionic conductivity due to the irreversible reactions.
 [DOI: 10.1149/1945-7111/acee24]

Manuscript submitted March 7, 2023; revised manuscript received June 26, 2023. Published August 25, 2023.

Supplementary material for this article is available online

Nowadays, Li-ion batteries (LIBs) have become part of daily life with billions used in electronic devices and electric vehicles. As conventional LIBs utilize flammable liquid electrolytes, increasing efforts are being invested to develop all-solid-state batteries (ASSBs) employing less or non-flammable solid-state electrolytes (SSEs).[1–4] Moreover, SSEs can also enable anode materials with higher capacity like Si and Li.[5–8] Unlike conventional LIBs, whose manufacturing process has been very well developed, there are still plenty of challenges when fabricating all-solid-state Li batteries (ASSLBs) on a commercial scale. The use of dry rooms is already well established for LIBs so it would be ideal if ASSLBs could also be made in the same facilities. Therefore, it is important to validate whether SSEs are stable in dry room conditions, however, the dry room stability of many SSEs has yet to be properly evaluated.

Most inorganic SSEs for ASSLBs can be grouped into three categories: oxides, sulfides, and halides.[9] Although oxide SSEs possess superior chemical and electrochemical stability, their high synthesis temperature and high Young's modulus limit their use in many applications.[9–12] Sulfide SSEs are frequently utilized in ASSLBs due to their high ionic conductivity, ease of synthesis, and high elemental abundance. However, sulfide electrolytes exhibit a narrow electrochemical stability window, leading to limited applications with cathode materials requiring a high cut-off voltage ($LiNi_{0.5}Mn_{1.5}O_2$) or large surface area ($LiFePO_4$) due to excessive sulfide oxidation and cathode electrolyte interphase (CEI) formation. Chlorides SSEs possess a higher oxidation stability so they can be employed when a high cut-off voltage is required at the cathode side.[13,14]

Several chlorides with the general formula $Li_3MCl_6$ (M = $Tb^{3+}$, $Lu^{3+}$, $Y^{3+}$, and $Sc^{3+}$) have been reported in the 1990s.[15,16] Depending on the size of the $M^{3+}$ cation and the $Li^+$ distribution in the structure, these chlorides can crystallize in the trigonal ($P\bar{3}m1$), orthorhombic (*Pmna*), or monoclinic ($C2/m$) structures.[9,15] Halide SSEs started receiving renewed attention after Asano et al. reported that $Li_3YCl_6$ (LYC) and $Li_3YBr_6$ synthesized by a mechanochemical method, exhibited ionic conductivities of 0.51 and 1.7 mS $cm^{-1}$, respectively, much higher than those previously reported.[17] As the $Cl^-$ anion exhibits a higher oxidation stability than $S^{2-}$, chloride SSEs are more oxidatively stable than sulfide electrolytes. The oxidation electrochemical window can reach approximately 4.2 V for chlorides.[9,16,18,19] Unlike conventional synthesis methods using high-temperature solid-state reactions, various halide SSEs at metastable phases and different crystal structures can be prepared using a mechanochemical approach.[19] Moreover, such an approach can improve the ionic conductivity of halide SSEs by introducing disorders into the cation and anion sublattices.[9,20,21] Tuning the crystal structures and the concentration of Li ions by partial substitution of the central metal cations is another effective method to boost ionic conductivity. $Li_{3-x}M_{1-x}N_xCl_6$ (M = $Er^{3+}$, $Y^{3+}$, and $Yb^{3+}$; N = $Zr^{4+}$ and $Hf^{4+}$) electrolytes were reported to exhibit an enhanced ionic conductivity than the unsubstituted $Li_3MCl_6$ electrolytes due to the formation of new phases with a lower migration barrier for Li ions.[22,23] For example, Kwak et al. improved the ionic conductivity of $Li_2ZrCl_6$ (LZC) by $Fe^{3+}$ substitution, resulting from the increased concentration of $Li^+$.[21]

Despite their superior oxidation stability over sulfide SSEs, the adaptability of chloride SSEs to scalable manufacturing conditions needs to be evaluated. A recent study on the dry room compatibility of $Li_6PS_5Cl$ (LPSCl) has shown that LPSCl is prone to hydrolysis

[z]E-mail: jijang@eng.ucsd.edu; zhengchen@eng.ucsd.edu; shmeng@uchicago.edu

when exposed to moisture, but a maximum dew point of −40 °C is sufficient to minimize $H_2S$ evolution to prevent ionic conductivity loss and to ensure workers' safety.[24,25] Likewise, chloride SSEs have been known to be sensitive towards hydrolysis upon moisture exposure.[9,26,27] $Li_3InCl_6$ (LIC) has been reported to form stable hydrate upon storage in air, but it can be recovered by heating above 200 °C.[28] On the other hand, some chloride SSEs have been found to undergo either decomposition or severe hydrolysis when exposed to air. Therefore, the dry room compatibility of chloride SSEs should be evaluated to identify the most promising chemistry and suitable processing conditions for mass production.

This study aims to investigate the dry room compatibility of chloride SSEs where the obtained results can be used as criterion for material selection for future upscaling processes. Three promising chloride SSEs possessing high ionic conductivities at ambient temperature, e.g., LZC, LYC, and LIC, were chosen for this study. Prior to testing the dry room stability, all materials were first exposed to ambient air (air-Exp), containing a higher humidity level than dry rooms, to speed up degradation for the ease of mechanistic study. Afterward, the exposed samples were recovered and underwent heat treatment (air-HT) to evaluate recoverability of the initial material. The obtained results show that LZC underwent severe hydrolysis, while LYC and LIC underwent hydration. Only LIC was recoverable after the heat treatment, rendering it the most stable chloride SSE among the three. Finally, the three chloride SSEs were exposed to a dry room environment, with reduced moisture level, for 3 h. The exposed electrolytes were used as catholytes in NCM811|LiIn half cells and exhibited higher cell impedance and lower discharge capacity. Compared to LPSCl,[25] the chloride SSEs studied here are more sensitive to moisture exposure.

## Experimental

***Synthesis of chloride SSEs.***—All chloride SSEs were synthesized via a mechanochemical approach using a Retsch PM200 planetary ball-mill. Precursors, including LiCl (Sigma Aldrich), $ZrCl_4$ (Sigma Aldrich), $YCl_3$ (Alfa Aesar), and $InCl_3$ (Alfa Aesar), were stoichiometrically mixed with a mortar and a pestle, and 1.5 g of precursor mixture were transferred to a 50 ml air-tight $ZrO_2$ jar with fifteen 10 mm $ZrO_2$ milling media in an Ar-filled glovebox. LZC and LIC were ball-milled at 550 rpm for 3 h, and LYC was at 500 rpm for 1 h.

***Exposure and heat treatment of chloride SSEs.***—Air-Exp samples were prepared by placing 0.5 g of chloride SSEs evenly in a 125 ml wide-mouth glass jar in an Ar-filled glovebox and then transferring them to the antechamber with a total volume of 250 l. The chamber door was opened for 1 min to fill the antechamber with ambient air having a relative humidity between 45%–55%. After 24 h of exposure, the antechamber was vacuumed and purged with Ar, and the air-Exp samples were collected. The Air-HT samples were obtained by heating the Air-Exp samples in quartz tubes under a dynamic vacuum at assigned temperatures (LZC: 350 °C;[29] LYC: 550 °C;[17] LIC: 260 °C[30]). Dry room exposed samples were prepared by distributing multiple batches of 0.5 g SSEs on petri dishes in a dry room environment with a dew point of −60 °C for 3 h.

***Electrochemical characterization.***—To avoid air exposure, all cell fabrication and measurements were done in an Ar-filled glovebox. To obtain the ionic conductivity, 75 mg of chloride SSE was placed in a 10 mm PEEK die and pressed at 370 MPa using a pair of titanium plungers to obtain the pellet. The SSE thickness is estimated by measuring the length difference of the cell with and without the SSE pellet with a Vernier caliper. The cell was tightened to 75 MPa using a cell holder. Electrochemical impedance spectroscopy (EIS) measurements were performed from 1 MHz to 0.1 Hz, with an applied AC amplitude of 30 mV. The acquired Nyquist plots were analyzed with Z-View software. To obtain the electronic conductivity, a DC voltage of 0.5 V was applied to the SSE pellet and the residual current induced by the excitation pulse was recorded. To obtain the oxidation potential of the pristine and dry room exposed chloride SSEs, the powders were mixed with acetylene black (AB) at a weight ratio of 7:3 (SSE:AB) with mortar and pestle. LiIn anode was prepared by vortex mixing Li and In powder (MSE Supplies) at a weight ratio of 1:33. liIn alloy was used as both counter and reference electrode. Linear scan voltammetry (LSV) was conducted using SSE-C | LPSCl | LiIn cells at a scan rate of 0.1 mV $s^{-1}$ from open circuit voltage (OCV) to 5 V vs Li/$Li^+$. The measurements were conducted using a Solartron 1260 Impedance Analyzer at room temperature.

Half cells were employed to evaluate the electrochemical performance of chloride SSEs (LZC, LYC, and LIC) before and after exposure to the dry room environment. The half cells were constructed by pelletizing 15 mg of NCM811 cathode composites, 70 mg of LPSCl and 50 mg of LiIn alloy anode with PEEK dies. The cathode composites were fabricated by mixing $LiNi_{0.8}Co_{0.1}Mn_{0.1}O_2$ (NCM811, LG Energy Solution), chloride SSEs, and vapor grown carbon fiber (VGCF, Sigma-Aldrich) at a weight ratio of 66:31:3 with mortar and pestle. The half cells were tested using Neware Battery cyclers (A211-BTS-1U-ZWJ) with cut-off voltages of 2.5 V and 4.3 V vs Li/$Li^+$ at room temperature. The cells underwent two formation cycles at C/10 (1 C = 200 mAh $g^{-1}$) and EIS were recorded in the second formation discharge at 50% state of charge. Afterward, the cells were cycled at C/3 with an additional constant voltage cut-off of C/10 at the end of charging for 50 cycles. Subsequently, the cells were again cycled at C/10 and the other EIS was recorded when discharged to a state-of-charge of 50%.

***Characterization.***—X-ray diffraction (XRD) patterns of chloride SSEs were obtained using a Bruker APEX II. The powder was sealed in a 0.7 mm boron-rich glass capillary in an Ar-filled glovebox. Measurements were taken using Mo K$\alpha$ radiation ($\lambda$ = 0.70926 Å) over a 2$\theta$ range of 5° to 40°, with a step size of 0.01°. Le Bail refinement was done using FullProf software. Space group $P-3m1$ was selected to refine LZC and LYC, and $C2/m$ was selected for LIC.[9,29,31,32] Energy dispersive X-ray spectroscopy (EDS) was obtained with a FEI Scios DualBeam Focused ion beam/scanning electron microscope, and the samples were prepared in an Ar-filled glovebox and transferred with an air-tight loader to avoid any atmosphere exposure. A NETZSCH STA 449 F3 Jupiter Simultaneous Thermal Analyzer with Coupled QMS 403 D Aëolos Mass Spectrometer was used to obtain thermogravimetric analysis/differential scanning calorimetry coupled mass spectrum data (TGA/DSC–MS). To observe $H_2O$ and HCl evolution, MS was set to monitor molecular weights at 18 and 36 g·$mol^{-1}$. 15–20 mg of chloride SSE samples were placed in $Al_2O_3$ pans (6.8 mm in diameter/85 $\mu$L). The samples were prepared within 2 min to minimize air exposure. All measurements were conducted in an $N_2$ atmosphere, scanning from 30 to 450 °C at a scan rate of 5 °C $min^{-1}$.

## Results and Discussion

To understand the impact of moisture exposure and potential recoverability, pure phase LZC, LYC, and LIC (confirmed with Le Bail refinement in Fig. S1) were exposed to ambient air followed by heat treatment. EIS at each stage was measured and is shown in Fig. 1. Before the exposure, all three materials exhibited ionic conductivities in the range of $10^{-4}$ S $cm^{-1}$, comparable to previous literature.[17,29,30] After the exposure, the ionic conductivities of the SSEs all dropped to $10^{-6}$ mS $cm^{-1}$ or lower, indicating some reaction has taken place. Note that the conductivity values only reflected the ionic conductivity of the decomposed or the hydrated products, rather than the degree of reactions. After heat treatment, only LIC recovered close to its pristine ionic conductivity, while both LZC and LYC exhibited further decay. The pristine and Air-Exp chloride SSEs exhibited similar electronic conductivities in the

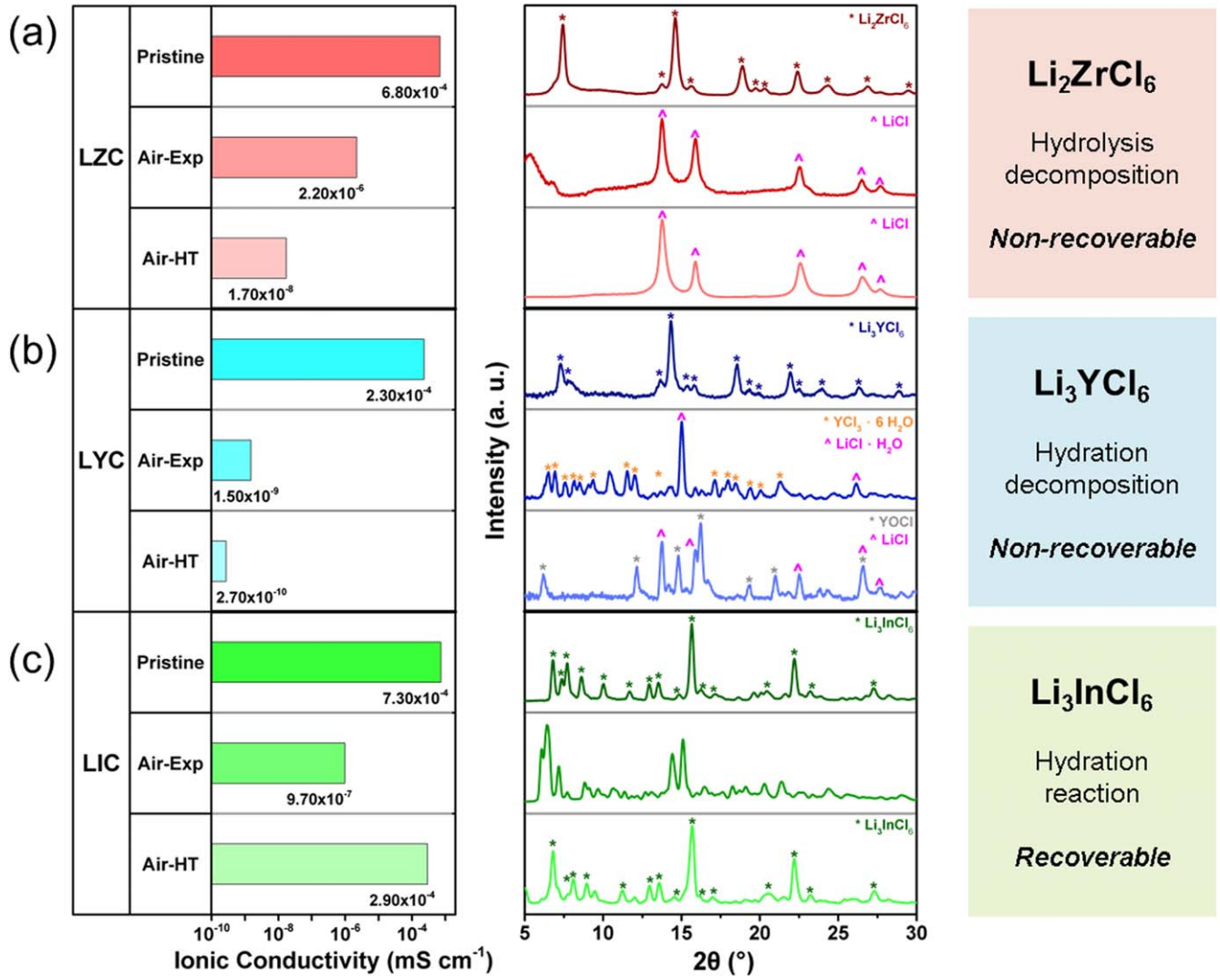


**Figure 1.** Ionic conductivities and XRD patterns of (a) LZC, (b) LYC, and (c) LIC before and after air exposure and after the heat treatment.

range of $10^{-9}$ S cm$^{-1}$ (Fig. S2), implying an electronically conductive phase was not formed after air exposure.

XRD patterns of all chloride SSE samples were investigated to understand the chemical reactions occurring during the moisture exposure and heat treatment. The XRD patterns showed that all three materials were fully or close to fully decomposed or hydrated, as the peaks of their pristine states were not observed. After exposing, the XRD pattern of LZC showed the formation of LiCl. The pattern remained similar after the heat treatment, suggesting that the Air-Exp LZC cannot be recovered. As $ZrCl_4$, one of its precursors, has high tendency to hydrolyze and form $ZrO_2$, it is likely to present in Air-Exp LZC.[33] Since $ZrO_2$ exhibited diffraction peaks with similar diffraction angles to those of LiCl (Fig. S3), EDS was employed to inspect the elemental ratio and the spectra are shown in Fig. S4.[34,35] The oxygen atomic ratio increased significantly to 43.2% after the air exposure and heat treatment, indicating that LZC chemically reacted with air. As Air-HT LZC exhibited an approximate atomic ratio of Zr:Cl:O = 1:2:2, the net chemical reaction after the exposure can be deduced:

$$Li_2ZrCl_6 + 2\,H_2O \rightarrow 2\,LiCl + ZrO_2 + 4\,HCl \quad [1]$$

The XRD pattern of Air-Exp LYC can be deconvoluted into $YCl_3{\cdot}6H_2O$ and $LiCl{\cdot}H_2O$ (Fig. S5), indicating that LYC decomposed into the hydrates of its precursors upon contact with air.[36,37] The chemical reaction can be written as:

$$Li_3YCl_6 + 9\,H_2O \rightarrow YCl_3 \cdot 6\,H_2O + 3\,LiCl \cdot H_2O \quad [2]$$

While anhydrous LiCl can easily be obtained by heating $LiCl{\cdot}H_2O$, $YCl_3{\cdot}6H_2O$ underwent a hydrolysis reaction to form YOCl.[27,38–40] Consequently, LiCl and YOCl were observed in the XRD pattern (Fig. S6) showing that LYC was not recoverable after heat treatment (Note S1).[34,40,41]

$$YCl_3 \cdot 6H_2O + 3\,LiCl \cdot H_2O \rightarrow YOCl + 3\,LiCl + 8\,H_2O + 2\,HCl \quad [3]$$

Unlike LZC and LYC, LIC can form stable hydrates without significant decomposition.[28,30] It can be restored to its original phase after heating at 260 °C, as shown in the XRD patterns in Fig. 1c. Nevertheless, formation of minuscule $In_2O_3$, resulting from slight hydrolysis, was reported due to weak acidity of $In^{3+}$ in aqueous solution, resembling the property of its $InCl_3$ precursor.[42]

Since HCl and $H_2O$ evolution is a key indication of hydrolysis and dehydration reactions, it is important to detect them directly. However, HCl and $H_2O$ are volatile and cannot be observed using XRD. TGA/DSC–MS was used to monitor both the weight change and gas evolution of the samples during the thermal treatment at high temperatures. The TGA/DSC–MS results of the three chloride SSEs at the pristine (Fig. S7) and air-exposed (Fig. 2) states were examined. At the pristine state, significant weight losses were only

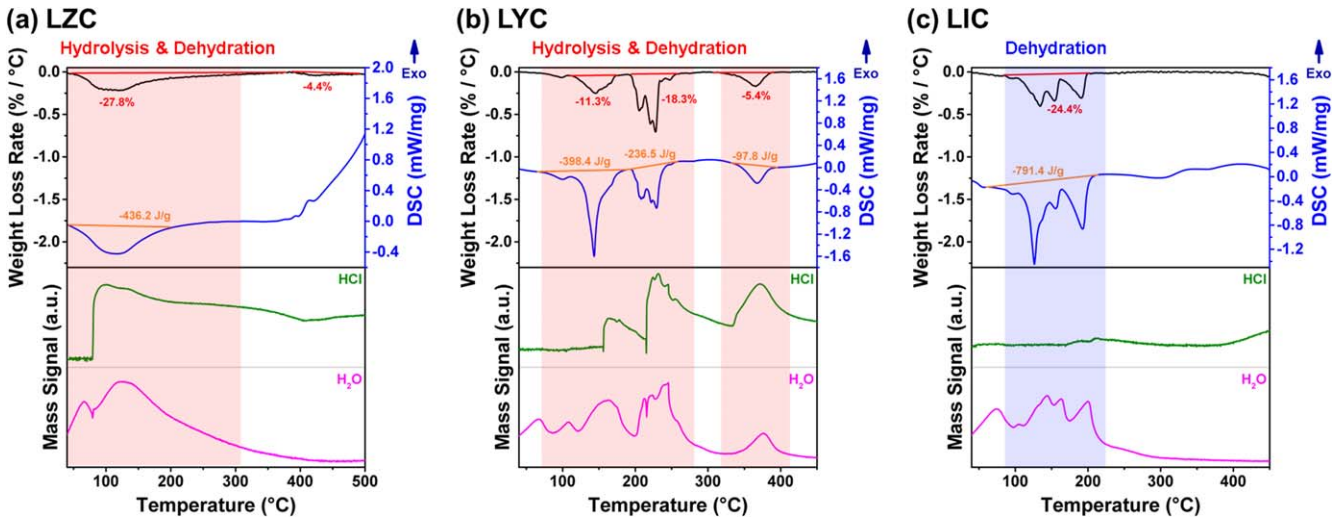


**Figure 2.** The TGA/DSC—MS of air-exposed (a) LZC, (b) LYC, and (c) LIC. HCl and $H_2O$ were monitored, as they are the product of hydrolysis and dehydration reactions, respectively.

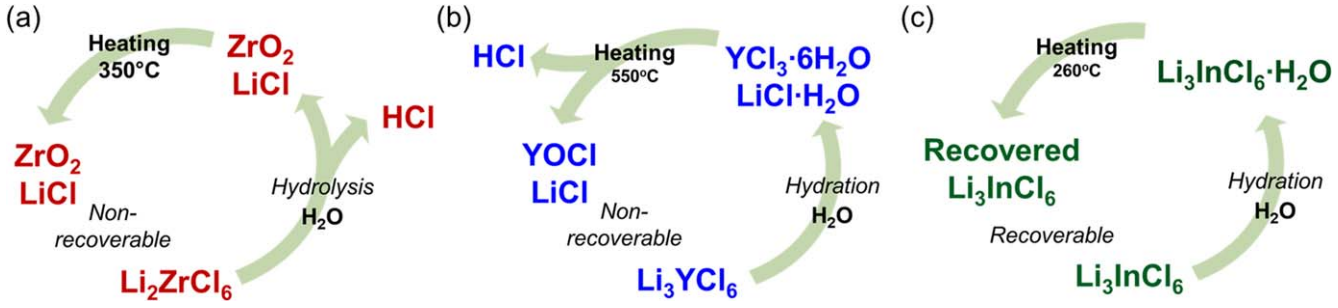


**Figure 3.** Summarized scheme of moisture stability and recovery process of (a) $Li_2ZrCl_6$, (b) $Li_3YCl_6$, and (c) $Li_3InCl_6$.

observed in pristine LZC above 350 °C, due to the sublimation of $ZrCl_4$.[43] All the other minor weight losses and gas evolution were a result of short air exposure during the sample preparation. After 24 h of air exposure, all three exhibited endothermic signals due to the dehydration reaction or desorption of $H_2O$. Air-Exp LZC released HCl when heated to 80 °C, indicating that the hydrolysis reaction started close to room temperature. As LZC was fully hydrolyzed, $ZrCl_4$ sublimation signals were no longer observed above 350 °C. Different from LZC, Air-Exp LYC did not have HCl evolution before 150 °C, indicating that $Li_3YCl_3$ hydrate was stable and started to hydrolyze and formed YOCl after 150 °C. No obvious HCl evolution was observed in Air-Exp LIC and $H_2O$ evolution ends at approximately 230 °C, in consistent with the recovery of the LIC phase after heat treatment at 260 °C observed in the XRD result.

To verify the chemical reaction deduced from the XRD result, the weight changes after air exposure and TGA (heat treatment), and net weight change are summarized in Table S1. To calculate the theoretical weight change, the molar mass of pristine SSEs and solid products (i.e., ignoring HCl and $H_2O$) are calculated. The theoretical values of the three SSEs can be obtained following Table S2. LZC exhibited a negative weight change of −4.3% after the exposure, indicating that it started to hydrolyze and gave off HCl upon contacting moisture. A further weight change of −32.2% was observed during the TGA, because of HCl and $H_2O$ removal. This led to a net weight loss of −35.1%, which is close to the theoretical value of −34.6%. LYC gained 36.5% weight during air exposure and lost 35.0% weight in TGA, leading to a net weight change of −11.3%. The difference between the experimental and theoretical value (−17.0%) could result from sample inhomogeneity during air exposure. LIC gained 28.1% after air exposure and lost 24.4% in TGA, resulting in a net change of −3.2%, close to the theoretical value of 0%. The weight analysis results are overall consistent with the XRD results. Based on the XRD and TGA/DSC–MS results, the chemical evolutions of the three chloride SSEs during air exposure and heat treatment can be summarized in Fig. 3.

Lastly, all SSEs were exposed to a dry room environment with a dew point of −60 °C for 3 h. Figure S8 presents the ionic conductivity changes and XRD patterns of the SSEs before and after dry room exposure. The ionic conductivities of all the SSEs dropped to approximately a quarter of their original values despite little to no change observed in their XRD patterns. The oxidation potential of the chloride SSEs after exposure to dry room was probed with LSV (Fig. S9). The oxidation onset voltages were all approximately 4 V, which is close to the theoretical calculation.[19] The oxidation onsets remained almost the same after the dry room exposure, as only $Cl^-$ is involved in the oxidation reaction ($2Cl^- \rightarrow Cl_2 + 2e^-$),[9] suggesting that the effect of hydration on the electrochemical window is minimal. To evaluate the electrochemical performance of the SSEs, they were paired with NCM811 cathode composites and assembled into NCM811-chloride SSE|LPSCl|LiIn half cells. Figure 4 presents the cycling performance and impedance changes before and after 50 cycles (Detailed fitting results are shown in Fig. S10). After dry room exposure, the impedance of the cells increased, especially the charge transfer impedance, indicating the decomposed products have negative impact to the electrochemical performance. The larger cell impedance resulted in more polarization and longer constant voltage capacities at the end of charging (Fig. S11). Consequently, NCM811 half cells using dry room exposed SSEs exhibited reduced capacities. The dry room exposed LZC cell exhibited the least capacity drop compared to its pristine

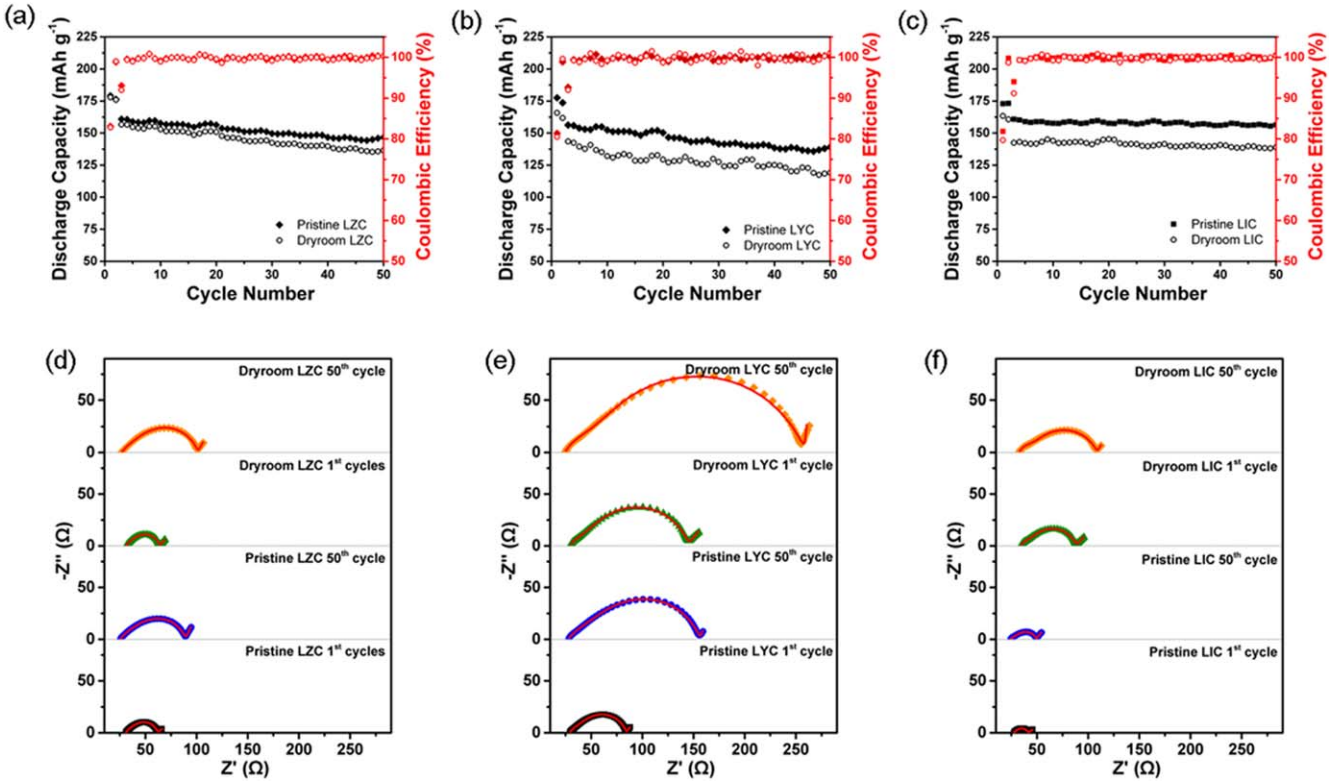


**Figure 4.** (a), (b), (c) Cycle performance and (d), (e), (f) corresponding impedance changes of NCM | Li-In half-cells whose cathode composites contain pristine and dry-room-exposed LZC, LYC, and LIC as catholytes.

form among the three SSEs, as the EIS had relatively minor degradation after the dry room exposure (Fig. 4d). The LYC cell exhibited the worst capacity retention among the three SSEs, as the dry room exposed LYC also exhibited the lowest ionic conductivity of $6.4 \times 10^{-5}$ S cm$^{-1}$ (Fig. S8a). A slight further capacity reduction can be observed in all cells, possibly because of contact loss or cathode electrolyte interphase formation, and it was reflected in the impedance increase shown in the Nyquist plots.[44,45]

## Conclusions

In this study, three chloride SSEs, namely LZC, LYC, and LIC, were synthesized and their chemical evolution during air exposure and heat treatment was analyzed using EIS, XRD, and TGA/DSC–MS. The experimental analysis indicates that the chloride SSEs suffer from different decomposition in moisture atmosphere depending on its metal center. Firstly, LZC hydrolyzes into $ZrO_2$ and LiCl upon contacting moisture and is not recoverable after heat treatment. Secondly, LYC decomposes into $YCl_3{\cdot}6H_2O$ and $LiCl{\cdot}H_2O$ during the exposure and $YCl_3$ further hydrolyzes to form YOCl, making LYC unrecoverable. Lastly, LIC forms a stable hydrate and can be easily recovered when heated to 260 °C to remove hydrated water. Finally, all three materials were exposed to a dry room environment with a dew point of −60 °C for three hours. Subsequent electrochemical tests indicate that all SSEs suffer from ionic conductivity decay, which is reflected in the reduced discharge capacity of NCM811|LiIn half cells. The SSEs evaluated here are sensitive to moisture even in dry room conditions. Nevertheless, surface modifications or doping can be explored to increase the moisture tolerance of chloride SSEs.

## Acknowledgments

This work was partially supported by LG Energy Solution through the Frontier Research Laboratory (FRL) program. Part of this work was performed at the San Diego Nanotechnology Infrastructure (SDNI) of the UCSD, a member of the National Nanotechnology Coordinated Infrastructure, supported by the National Science Foundation (Grant ECCS-1542148). The authors acknowledge the use of facilities and instrumentation at the UC Irvine Materials Research Institute (IMRI) supported in part by the National Science Foundation Materials Research Science and Engineering Center program through the UC Irvine Center for Complex and Active Materials (DMR-2011967).

## ORCID

Yu-Ting Chen https://orcid.org/0000-0001-9525-8407
Jeong Beom Lee https://orcid.org/0000-0001-6221-4037
Long Hoang Bao Nguyen https://orcid.org/0000-0001-7823-1595
Zheng Chen https://orcid.org/0000-0002-9186-4298
Ying Shirley Meng https://orcid.org/0000-0001-8936-8845

## References

1. Y. Horowitz, C. Schmidt, D.-H. Yoon, L. M. Riegger, L. Katzenmeier, G. M. Bosch, M. Noked, Y. Ein-Eli, J. Janek, and W. G. Zeier, "Between liquid and all solid: a prospect on electrolyte future in lithium-ion batteries for electric vehicles." *Energy Technology*, **8**, 2000580 (2020).
2. Y. S. Jung, D. Y. Oh, Y. J. Nam, and K. H. Park, "Issues and challenges for bulk-type all-solid-state rechargeable lithium batteries using sulfide solid electrolytes." *Isr. J. Chem.*, **55**, 472 (2015).
3. K. Kerman, A. Luntz, V. Viswanathan, Y.-M. Chiang, and Z. Chen, "practical challenges hindering the development of solid state Li ion batteries." *J. Electrochem. Soc.*, **164**, A1731 (2017).
4. H. Lee, P. Oh, J. Kim, H. Cha, S. Chae, S. Lee, and J. Cho, "Advances and prospects of sulfide all-solid-state lithium batteries via one-to-one comparison with conventional liquid lithium ion batteries." *Adv. Mater.*, **31**, 1900376 (2019).
5. D. H. Tan, Y.-T. Chen, H. Yang, W. Bao, B. Sreenarayanan, J.-M. Doux, W. Li, B. Lu, S.-Y. Ham, and B. Sayahpour, "Carbon free high loading silicon anodes enabled by sulfide solid electrolytes for robust all solid-state." *Batteries. arXiv preprint arXiv*, **2103**, 04230 (2021).
6. H. Huo and J. r. Janek, "Silicon as emerging anode in solid-state batteries." *ACS Energy Lett.*, **7**, 4005 (2022).
7. S. Cangaz, F. Hippauf, F. S. Reuter, S. Doerfler, T. Abendroth, H. Althues, and S. Kaskel, "Enabling high-energy solid-state batteries with stable anode interphase by the use of columnar silicon anodes." *Adv. Energy Mater.*, **10**, 2001320 (2020).

8. S.-Y. Ham, H. Yang, O. Nunez-cuacuas, D. H. Tan, Y.-T. Chen, G. Deysher, A. Cronk, P. Ridley, J.-M. Doux, and E. A. Wu, "Assessing the critical current density of all-solid-state Li metal symmetric and full cells." *Energy Storage Mater.*, **55**, 455 (2023).
9. H. Kwak, S. Wang, J. Park, Y. Liu, K. T. Kim, Y. Choi, Y. Mo, and Y. S. Jung, "Emerging Halide superionic conductors for all-solid-state batteries: design, synthesis, and practical applications." *ACS Energy Lett.*, **7**, 1776 (2022).
10. K. H. Park, Q. Bai, D. H. Kim, D. Y. Oh, Y. Zhu, Y. Mo, and Y. S. Jung, "Design strategies, practical considerations, and new solution processes of sulfide solid electrolytes for all-solid-state batteries." *Adv. Energy Mater.*, **8**, 1800035 (2018).
11. K. J. Kim, M. Balaish, M. Wadaguchi, L. Kong, and J. L. Rupp, "Solid-state Li–metal batteries: challenges and horizons of oxide and sulfide solid electrolytes and their interfaces." *Adv. Energy Mater.*, **11**, 2002689 (2021).
12. K. H. Kim, Y. Iriyama, K. Yamamoto, S. Kumazaki, T. Asaka, K. Tanabe, C. A. Fisher, T. Hirayama, R. Murugan, and Z. Ogumi, "Characterization of the interface between LiCoO2 and Li7La3Zr2O12 in an all-solid-state rechargeable lithium battery." *J. Power Sources*, **196**, 764 (2011).
13. J. Jang, Y.-T. Chen, G. Deysher, D. Cheng, S.-Y. Ham, A. Cronk, P. Ridley, H. Yang, B. Sayahpour, and B. Han, "Enabling a co-free, high-voltage LiNi0. 5Mn1. 5O4 cathode in all-solid-state batteries with a halide electrolyte." *ACS Energy Lett.*, **7**, 2531 (2022).
14. A. Cronk, Y.-T. Chen, G. Deysher, S.-Y. Ham, H. Yang, P. Ridley, B. Sayahpour, L. H. B. Nguyen, J. A. S. Oh, and J. Jang, "Overcoming the interfacial challenges of LiFePO4 in inorganic all-solid-state." *Batteries.*, **8**, 827 (2022).
15. A. Bohnsack, F. Stenzel, A. Zajonc, G. Balzer, M. S. Wickleder, and G. Meyer, "Ternäre halogenide vom Typ A3MX6. VI [1]. Ternäre chloride der selten-erd-elemente mit lithium, Li3MCl6 (M=Tb— Lu, Y, Sc): synthese, kristallstrukturen *u*nd ionenbewegung." *Z. Anorg. Allg. Chem.*, **623**, 1067 (1997).
16. X. Li, J. Liang, X. Yang, K. R. Adair, C. Wang, F. Zhao, and X. Sun, "Progress and perspectives on halide lithium conductors for all-solid-state lithium batteries." *Energy Environ. Sci.*, **13**, 1429 (2020).
17. T. Asano, A. Sakai, S. Ouchi, M. Sakaida, A. Miyazaki, and S. Hasegawa, "Solid halide electrolytes with high lithium-ion conductivity for application in 4 v class bulk-type all-solid-state batteries." *Adv. Mater.*, **30**, 1803075 (2018).
18. K. Kim, D. Park, H.-G. Jung, K. Y. Chung, J. H. Shim, B. C. Wood, and S. Yu, "Material design strategy for halide solid electrolytes Li3MX6 (X=Cl, Br, and I) for all-solid-state high-voltage Li-ion batteries." *Chem. Mater.*, **33**, 3669 (2021).
19. S. Wang, Q. Bai, A. M. Nolan, Y. Liu, S. Gong, Q. Sun, and Y. Mo, "Lithium Chlorides and Bromides as Promising Solid-State Chemistries for Fast Ion Conductors with Good Electrochemical Stability." *Angew. Chem. Int. Ed.*, **58**, 8039 (2019).
20. R. Schlem, S. Muy, N. Prinz, A. Banik, Y. Shao-Horn, M. Zobel, and W. G. Zeier, "Mechanochemical synthesis: a tool to tune cation site disorder and ionic transport properties of Li3MCl6 (M= Y, Er) superionic conductors." *Adv. Energy Mater.*, **10**, 1903719 (2020).
21. H. Kwak, D. Han, J. Lyoo, J. Park, S. H. Jung, Y. Han, G. Kwon, H. Kim, S. T. Hong, and K. W. Nam, "New cost-effective halide solid electrolytes for all-solid-state batteries: mechanochemically prepared Fe3+-Substituted Li2ZrCl6." *Adv. Energy Mater.*, **11**, 2003190 (2021).
22. J. Park, D. Han, H. Kwak, Y. Han, Y. J. Choi, K.-W. Nam, and Y. S. Jung, "Heat treatment protocol for modulating ionic conductivity via structural evolution of Li3-xYb1-xMxCl6 (M=Hf4+, Zr4+) new halide superionic conductors for all-solid-state batteries." *Chem. Eng. J.*, **425**, 130630 (2021).
23. K.-H. Park, K. Kaup, A. Assoud, Q. Zhang, X. Wu, and L. F. Nazar, "High-voltage superionic halide solid electrolytes for all-solid-state Li-ion batteries." *ACS Energy Lett.*, **5**, 533 (2020).
24. C. l Singer, H.-C. Töpper, T. Kutsch, R. Schuster, R. Koerver, and R. d. Daub, "Hydrolysis of argyrodite sulfide-based separator sheets for industrial all-solid-state battery production." *ACS Applied Materials & Interfaces*, **14**, 24245 (2022).
25. Y.-T. Chen, M. A. Marple, D. H. Tan, S.-Y. Ham, B. Sayahpour, W.-K. Li, H. Yang, J. B. Lee, H. J. Hah, and E. A. Wu, "Investigating dry room compatibility of sulfide solid-state electrolytes for scalable manufacturing." *J. Mater. Chem. A*, **10**, 7155 (2022).
26. X. Li, J. Liang, K. R. Adair, J. Li, W. Li, F. Zhao, Y. Hu, T.-K. Sham, L. Zhang, and S. Zhao, "Origin of Superionic Li3Y1–x In x Cl6 halide solid electrolytes with high humidity tolerance." *Nano Lett.*, **20**, 4384 (2020).
27. M. D. Taylor, "Preparation of anhydrous lanthanon halides." *Chem. Rev.*, **62**, 503 (1962).
28. W. Li, J. Liang, M. Li, K. R. Adair, X. Li, Y. Hu, Q. Xiao, R. Feng, R. Li, and L. Zhang, "Unraveling the origin of moisture stability of halide solid-state electrolytes by in situ and operando synchrotron X-ray analytical techniques." *Chem. Mater.*, **32**, 7019 (2020).
29. K. Wang, Q. Ren, Z. Gu, C. Duan, J. Wang, F. Zhu, Y. Fu, J. Hao, J. Zhu, and L. He, "A cost-effective and humidity-tolerant chloride solid electrolyte for lithium batteries." *Nat. Commun.*, **12**, 1 (2021).
30. X. Li, J. Liang, J. Luo, M. N. Banis, C. Wang, W. Li, S. Deng, C. Yu, F. Zhao, and Y. Hu, "Air-stable Li 3 InCl 6 electrolyte with high voltage compatibility for all-solid-state batteries." *Energy Environ. Sci.*, **12**, 2665 (2019).
31. M. O. Schmidt, M. S. Wickleder, and G. Meyer, "Zur kristallstruktur von Li3InCl6." *Z. Anorg. Allg. Chem.*, **625**, 539 (1999).
32. R. Schlem, A. Banik, S. Ohno, E. Suard, and W. G. Zeier, "Insights into the lithium sub-structure of superionic conductors Li3YCl6 and Li3YBr6." *Chem. Mater.*, **33**, 327 (2021).
33. Z. Fang and D. A. Dixon, "Hydrolysis of ZrCl4 and HfCl4: The initial steps in the high-temperature oxidation of metal chlorides to produce ZrO2 and HfO2." *The Journal of Physical Chemistry C*, **117**, 7459 (2013).
34. A. Ievinš, M. Straumanis, and K. Karlson, "Präzisionsbestimmung von gitterkonstanten hygroskopischer verbindungen (LiCl, NaBr)." *Z. Phys. Chem.*, **40**, 146 (1938).
35. B. Bondars, G. Heidemane, J. Grabis, K. Laschke, H. Boysen, J. Schneider, and F. Frey, "Powder diffraction investigations of plasma sprayed zirconia." *J. Mater. Sci.*, **30**, 1621 (1995).
36. A. Bell and A. Smith, "Structure of hexaaquadichloroyttrium (III) chloride." *Acta Crystallogr., Sect. C: Cryst. Struct. Commun.*, **46**, 960 (1990).
37. A. Hönnerscheid, J. Nuss, C. Mühle, and M. Jansen, "Die kristallstrukturen der monohydrate von lithiumchlorid *u*nd lithiumbromid." *Z. Anorg. Allg. Chem.*, **629**, 312 (2003).
38. G. Meyer, E. Garcia, and J. D. Corbett, "The ammonium chloride route to anhydrous rare Earth chlorides—The example of YCl3." *Inorg. Synth.*, **25**, 146 (1989).
39. C. Wang, J. Liang, J. Luo, J. Liu, X. Li, F. Zhao, R. Li, H. Huang, S. Zhao, and L. Zhang, "A universal wet-chemistry synthesis of solid-state halide electrolytes for all-solid-state lithium-metal batteries." *Sci. Adv.*, **7**, eabh1896 (2021).
40. G. Meyer and P. Ax, "An analysis of the ammonium chloride route to anhydrous rare-Earth metal chlorides." *Mater. Res. Bull.*, **17**, 1447 (1982).
41. G. Meyer and T. Staffel, "Die Tieftemperatur-Synthese von Oxidhalogeniden, YOX (X=Cl, Br, I), als Quelle der Verunreinigung von Yttriumtrihalogeniden, YX3, bei der Gewinnung nach der Ammoniumhalogenid-Methode. Die Analogie von YOCl *u*nd YSCl." *Z. Anorg. Allg. Chem.*, **532**, 31 (1986).
42. S. Wang, X. Xu, C. Cui, C. Zeng, J. Liang, J. Fu, R. Zhang, T. Zhai, and H. Li, "Air sensitivity and degradation evolution of halide solid state electrolytes upon exposure." *Adv. Funct. Mater.*, **32**, 2108805 (2022).
43. J. H. Shin, M. S. Choi, D. J. Min, and J. H. Park, "Isothermal and non-isothermal sublimation kinetics of zirconium tetrachloride (ZrCl4) for producing nuclear grade Zr." *Mater. Chem. Phys.*, **143**, 1075 (2014).
44. R. Koerver, I. Aygün, T. Leichtweiß, C. Dietrich, W. Zhang, J. O. Binder, P. Hartmann, W. G. Zeier, and J. Janek, "Capacity fade in solid-state batteries: interphase formation and chemomechanical processes in nickel-rich layered oxide cathodes and lithium thiophosphate solid electrolytes." *Chem. Mater.*, **29**, 5574 (2017).
45. T. Shi, Y.-Q. Zhang, Q. Tu, Y. Wang, M. Scott, and G. Ceder, "Characterization of mechanical degradation in an all-solid-state battery cathode." *J. Mater. Chem. A*, **8**, 17399 (2020).